ISSN 1855-9913

Journal of the Laser and Health Academy
Vol. 2012, No.1; www.laserandhealth.com

Combined Fractional and Bulk Heating Modality for Nd:YAG Laser Skin Treatments

Mark B Taylor[1] ,Matjaz Lukac,[2] Martin Gorjan,[3] Karolj Nemes,[3]

[1]Gateway Aesthetic Institute & Laser Center, 440 West 200 South, Salt Lake City, Utah, USA
[2]Jozef Stefan Institute, Complex Matter Dept., Jamova 39, Ljubljana, Slovenia
[3]Fotona d.d., Stegne 7, Ljubljana, Slovenia

ABSTRACT

For deeply penetrating laser wavelengths, such as 1064 nm, the effect of light scattering in the skin leads to a spreading of the beam and consequently a significant reduction in effective fluence for small laser-beam spot sizes. For this reason, the 1064 nm Nd:YAG laser has not been used with fractional handpieces, where pixel beam spot sizes are typically very small. Instead, Nd:YAG fractional treatments are often performed using a special *FRAC3*®, self-induced 3-D fractional effect.

There are, however, certain Nd:YAG laser skin treatments, such as for resistant port wine stains and hemagiomas, that might benefit considerably by using a standard fractional beam technique. In this paper, we report on a recently introduced Nd:YAG laser scanner which operates at a fractional pixel size of 2 mm. Using a Monte Carlo numerical model, we show that this pixel size represents a suitable compromise between the effects of scattering and the desire to limit thermal effects to small pixel islands. We further show that scattering effects can be utilized to control the depth of the thermal fractional effect within the skin by varying the intra-spot pixel separation.

Key words: fractional skin rejuvenation, *FRAC3*, Nd:YAG laser, port wine stain, hemangioma.

Article: J. LAHA, Vol. 2012, No.1; pp. 26-34.
Received: April 13, 2012; Accepted: May 7, 2012

I. INTRODUCTION

Also known as fractional photothermolysis, fractional laser resurfacing is a relatively new method of skin rejuvenation [1, 2]. Unlike selective photothermolysis [3], where the whole of the selected target area is damaged, fractional photothermolysis seeks to only damage certain zones within the selected target area, producing tiny dot- or pixel-like treated areas in the skin. This leaves the other zones within the skin perfectly intact; hence only causing fractional damage through the heat of the light source. The skin heals much faster than if the whole area was treated, as the 'healthy' untreated tissue surrounding the treated zones helps to fill in the damaged area with new cells [2].

The concept of fractional photothermolysis can be applied with either ablative laser resurfacing or non-ablative laser skin rejuvenation, using the various different wavelengths of lasers available. Ablative fractional resurfacing is a treatment for fine and deep wrinkles, scar revision and superficial skin lesions [4]. Primarily used for the correction of moderate-to-deep wrinkles, this laser delivers micro-fractional columns of laser light to the outermost layers of the skin. This treatment works by using an ablative Er:YAG or CO_2 laser to create thousands of microscopic areas in which the top layer of the skin is ablated (removed) (See Fig. 1). Typical dimensions of the microscopic zones range between 0.25 and 0.5 mm [5, 6].

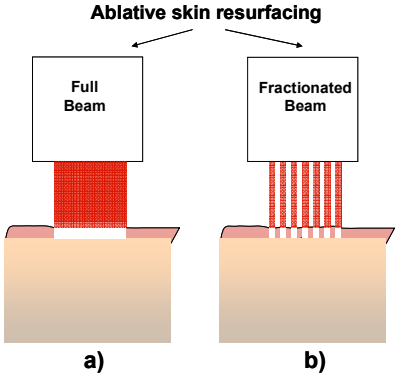

Fig. 1: a) Ablative full-beam skin resurfacing; b) ablative fractional skin resurfacing.

When compared to traditional, full-beam Er:YAG laser resurfacing, this approach produces similar results with far less downtime, and produces impressive changes in skin texture, wrinkle reduction, dark (sun) spots, and abnormal skin coloration [19-22].

In a non-ablative regime, fractional photothermolysis creates a two-dimensional matrix of columns of thermal damage that can, depending on the laser wavelength, extend deep into the dermis (See Fig. 2).

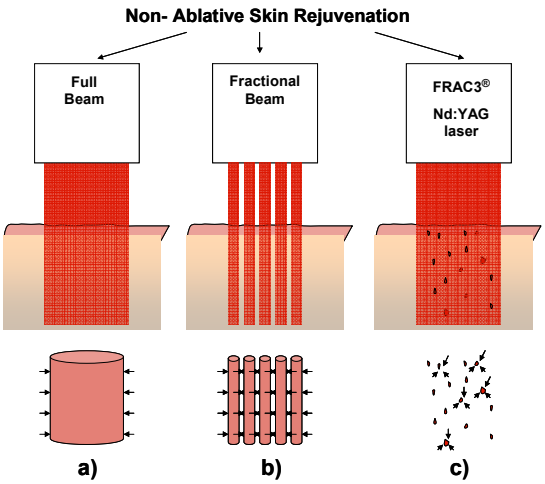

Fig. 2: a) Non-ablative full beam skin rejuvenation; b) non-ablative fractional skin rejuvenation; c) *FRAC3*® Nd:YAG laser non-ablative fractional skin rejuvenation.

Among non-ablative laser devices, the Nd:YAG laser holds the most prominent position due to its long wavelength (λ) of 1064 nm, which in terms of absorption lies in an optical window that allows light of this wavelength to penetrate deep into the dermis (up to 10 mm) (See Fig. 3).

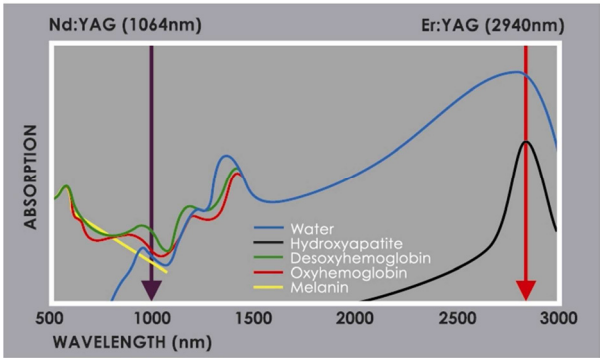

Fig. 3: The absorption coefficient in human tissues, μ_a as a function of laser wavelength. The absorption coefficient is at a minimum with the Nd:YAG laser wavelength (1.064 μm), and at a maximum with the Er:YAG laser wavelength (2.94 μm). Figure reprinted with permission from ref. 7.

For deeply penetrating laser wavelengths, such as 1064 nm, the effects of light scattering can be considerable [7]. This is because as a beam propagates into the skin, light scattering spreads the beam radially outward on each side, decreasing the beam's effective fluence as it penetrates into the skin. This effect is more pronounced in smaller spot sizes where the spreading of the beam is relatively large compared to the incoming beam spot size (See Fig. 4).

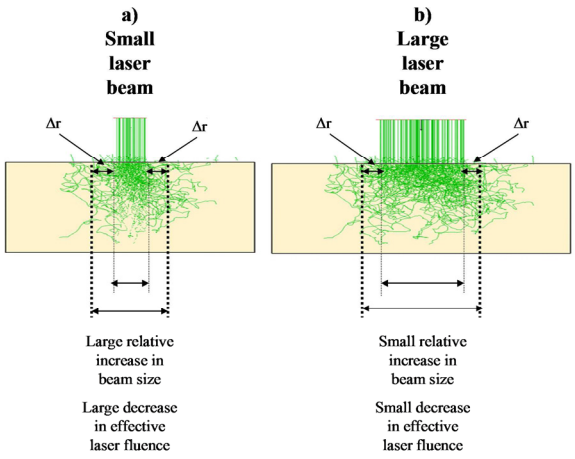

Fig. 4: Influence of scattering on the effective laser beam spot size. Figure reprinted with permission from ref. 7.

This is why, for example, the effective fluence within the skin of a 3 mm incoming Nd:YAG laser beam is 1.6 times smaller than the effective fluence of a 9 mm laser beam [7]. With fractional pixel sizes which are typically below 0.5 mm, the penetration depth of the Nd:YAG laser would be even smaller. For this reason, the 1064 nm Nd:YAG laser has been used primarily in the full-beam regime, while fractional treatments have been performed using a special *FRAC3*®, self-induced 3-D fractional effect [8-11]. This effect utilizes the Nd:YAG laser's high peak power and energy capabilities to create thermal effects only at areas of pre-existing skin damage. *FRAC3*® differs intrinsically from full-beam fractional technologies in which the beam itself is fractionated upon delivery. By contrast a *FRAC3*® beam is whole upon contact with the skin surface and the skin imperfections themselves induce the increased local absorption and scattering, resulting in a 3D fractional heat distribution precisely at the skin's imperfection targets (See Fig. 2c). The efficacy of *FRAC3*® rejuvenation has been demonstrated histologically, electron micrographically, through physiological measurements of skin parameters, through blinded assessment of before and after pictures, and by patient satisfaction. *FRAC3*® can be used to rejuvenate skin in every Fitzpatrick phototype [12].

There are, however, Nd:YAG laser skin treatments, such as treatments of resistant port wine stains and hemagiomas, that might benefit considerably by using a fractionated laser beam technique. In this paper, we report on a recently introduced Nd:YAG laser scanner, the Fotona S11 [13], that operates at a small pixel size of 2 mm. Using a Monte Carlo numerical model, we show that this pixel size represents a suitable compromise between the effects of scattering and the desire to reduce the damaged area of the skin by fractionated heating. We further show that scattering effects can be utilized to control the depth of the thermal fractional effect within the skin by varying the intra-spot pixel separation.

II. MATERIALS AND METHODS

a) Characteristics of the analyzed fractional device

The analyzed Nd:YAG fractional device was a Fotona S11 scanning handpiece with a 2 mm pixel size (See Fig. 5) [13].

Fig. 5: Non-ablative fractional Nd:YAG scanning handpiece (Fotona S11-F) [13].

The Fotona S11 fractional scanner uses a pixel spot size of d=2mm, and allows skin coverage to be adjusted over a wide range, from 100% (with intra-pixel separation of p=2mm), 63% (p=2.4mm), 53 % (p=2.6mm), 20% (p=3.9mm), 16% (p=4.5mm) and to 13% (p=4.9mm). See Figs. 6 and 7.

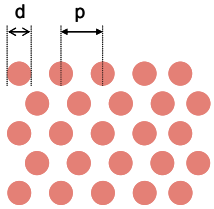

Fig. 6: The Fotona S11 non-ablative Nd:YAG scanning handpiece uses a fixed pixel size of d = 2 mm and allows the user to adjust the intra-pixel pitch (p) from 2 to 5.3 mm [13].

Figure 7 shows the calculated dependence of the skin coverage (in %) on the intra-pixel pitch.

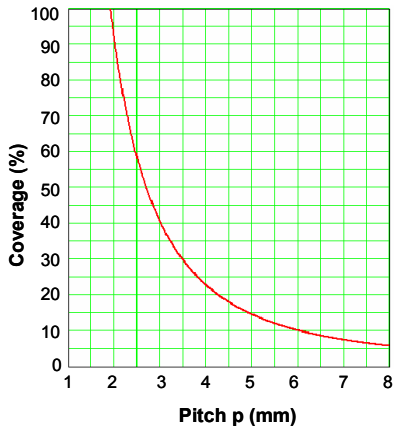

Fig. 7: Dependence of skin coverage on the intra-pixel pitch (p) for the 2 mm pixel size Fotona S11 scanner.

b) Skin Optics

The absorption in skin is mainly caused by water molecules, proteins and pigments [14]. Due to absorption, light intensity decreases with depth according to the Beer-Lambert law $I(z;\lambda) \alpha \exp(-\mu_a(\lambda)z)$, with the absorption coefficient μ_a being wavelength dependent.

Skin is also a heavy scatterer: its scattering coefficient μ_s being somewhere between 10 and 100 cm^{-1}. Due to its structural diversity, the contributions to scattering are twofold: atoms and molecules themselves scatter light according to Rayleigh theory, where the scattered intensity I_s is inversely proportional to the fourth power of the light's wavelength according to $I_S \alpha (1+\cos^2 \phi)/\lambda^4$, where ϕ is the deflection angle. The collagen fibers and other structures, having sizes comparable to light's wavelength, scatter the light according to Mie theory instead. The intensity of scattered light follows a much weaker wavelength dependence, $I_S \alpha \lambda^4$, λ being between 0.4 and 0.5; the scatter direction is mostly forward. The observed scattering in the skin is indeed mostly forward, but neither of the two theories adequately explain why this is so [15]. Many special empirical scattering (or phase) functions have been introduced instead to fit the measured data and describe the angular probability after the scattering "event". They can be used together with the scattering coefficient, stating the probability for the scattering event and the absorption coefficient, to model light propagation in the skin or other tissues [16].

c) Modeling light propagation

The most fundamental approach on calculating light's propagation is based on the physics of Maxwell's equations. However, because of the complexities involved, such an approach can be of limited applicability [15]. Due to its simplicity, universality and good practical results, photon transport theory is frequently used instead [14].

A beam of light is described with its radiance J (r, s), expressing the power at the position r flowing in the direction s. Radiance is governed by the radiative transport equation as follows:

$$dJ(r, s)/ds = -\mu_t J(r,s) + \mu_s \int p(s,s') J(r,s') d\Omega. \quad (1)$$

Radiance J(r, s) is being diminished proportionally to the total attenuation coefficient $\mu_t = \mu_a + \mu_s$ which is a sum of the absorption and scattering attenuation coefficients. On the other hand, radiance J(r, s) is being augmented by the light scattered from direction s' to direction s, the magnitude of which is described by the phase function p(s, s'). Commonly used is a Henyey-Greenstein phase function, which can be expressed as [16]:

$$p(s, s') = p(\phi) = (\mu_s/\mu_t) (1-g^2)/(1+g^2-2g\cos \phi)^{3/2}. \quad (2)$$

Depending on the average cosine or anisotropy factor g = cos ϕ: g = 1 denotes purely forward scattering, g = −1 purely backward and g = 0 isotropic scattering. Most tissues are mainly forward scattering; for skin, the anisotropy factor g was found to be between 0.8 and 0.9 [14, 15].

The radiative transport equation is difficult to solve directly, and many approximations exist, among others the Kubelka-Munk, inverse adding-doubling and the diffusion approximation. Since the mean free path of the light propagating in the skin is much smaller than the typical dimensions involved, propagation quickly becomes effectively random [16]. The Monte-Carlo simulation is then the preferred method for numerically solving the radiative transport problem [14, 15].

In a Monte-Carlo simulation the laser beam is represented as a stream of a large number N of "photons", each having a coordinate, direction and energy weight. Each photon is statistically ray-traced through tissue following five steps (depicted in Fig. 8):

i) Photon generation

The initial location and direction of propagation are randomly determined according the original beam.

ii) Pathway generation

The path to the next event is determined: the direction of propagation is determined according to the phase function p(ϕ). The traveled distance Δr is determined by choosing a random number ξ between 0 and 1 and using logarithmic distribution

$$\Delta r = - \log (\xi) / \mu_t \qquad (3)$$

iii) Absorption

The photon energy weight E is decreased after each event according to the absorption and scattering coefficient

$$\Delta E = - \mu_a / \mu_t \, E \qquad (4)$$

iv) Elimination

When the photon energy weight goes below some predetermined threshold, its propagation is terminated and a new photon is launched.

v) Detection

The absorbed energy ΔE is registered at the event coordinates after each event.

At the end of the procedure a three-dimensional distribution of absorbed energy is produced. More details about the Monte-Carlo algorithm implementation for light propagation through skin can be found in ref. 17 and 18.

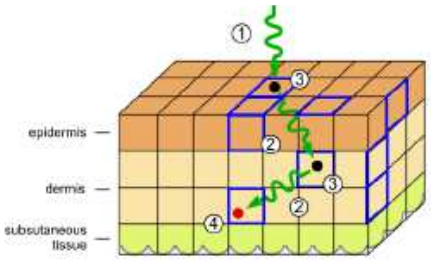

Fig 8: Schematic representation of a Monte-Carlo simulation of a laser beam propagating in skin. It consists of five steps (see text above): 1 - photon generation, 2 - pathway generation, 3 - absorption, 4 - elimination and 5 - detector count. Black dots represent scattering events and blue squares represent detector cell counts. The grid size is exaggerated for clarity.

We used an optical ray-tracing program Zemax EE, which features a highly efficient Monte-Carlo implementation, to obtain the distributions of absorbed light. Laser light was assumed to be directed perpendicularly to the skin surface. The simulation consisted of two layers of skin (epidermis and dermis) irradiated by laser beams of wavelength λ = 1064 nm. Distributions of absorbed light were calculated for various spot sizes of square (or "top-hat") collimated beams. We observed the absorbed energy densities at the surface and at a depth of z for each spot size and also for different intra-spot separations on the surface. Figure 9 shows a typical side view of a ray tracing calculation.

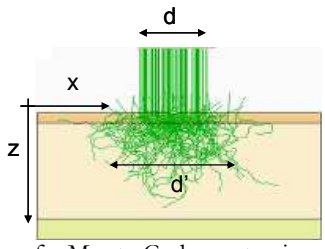

Fig. 9: Side view of a Monte Carlo ray tracing calculation for N = 100 photons. The initial spot size, d, of the incoming beam spreads to an effective spot size of d'.

Skin parameters used in our calculations are: μ_a = 0.041 cm^{-1}, μ_s = 100 cm^{-1}, and g = 0.87.

d) Modeling temperature distributions

In our model, it is assumed that the temperature increase immediately following a laser pulse is proportional to the absorbed laser beam energy within a particular skin volume. We assumed that within the dermis the heat diffusion away from the heated pixel island is not appreciable during the time it takes to complete a full scan. Thermal profiles resulting from individual neighboring laser pixels therefore overlap to form a joint thermal lattice within the skin.

III. RESULTS

a) Dependence of temperature profiles on fractional pixel size

Due to scattering, even a perfectly shaped laser beam, with a perfect, top-hat incoming beam profile of spot size d develops into a bell-shaped beam profile with spot size d' (d'>d), which increases as the beam penetrates deeper into the skin. As a result the spatial temperature distribution within a thermal island has a lower peak and longer tails. This can be seen in Fig. 10, which depicts the calculated profiles of the temperature increase, ΔT, for different incoming beam spot sizes (d) at a skin depth of z = 1 mm, and for the same incoming top-hat beam fluence (defined as laser pulse energy per beam area).

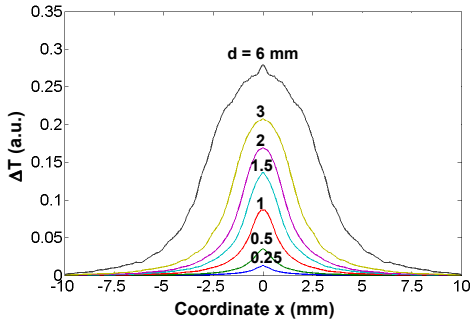

Fig. 10: Dependence of the spatial profiles of the temperature increase, ΔT on the incoming laser beam spot size at a skin depth of z = 1mm. For the definition of coordinates x and z, see Fig. 6.

Beam spreading and consequent reduction in the peak temperature are more pronounced for smaller incoming beam spot sizes. This can be seen from Fig. 11, which for the skin depth of z = 0.5 mm depicts the peak temperature increase ($\Delta T'_{max}$) for different spot sizes (d) of the incoming laser beam. The temperature increase, $\Delta T'_{max}$ is plotted relative to the temperature increase, ΔT_{max} for = 20 mm. The 20 mm spot size is chosen as it is considered to be large enough not to be influenced considerably by light scattering.

b) Dependence of temperature profiles on fractional pitch

When a matrix of laser pixels is deposited unto the skin, the absorption of laser light leads to a formation of a "temperature lattice" within the skin. When the chosen intra-pixel separation is small the temperature profiles of individual pixels may start to overlap as the individual laser beam columns propagate and broaden within the skin. This can be seen from Figs. 12 and 13 that show temperature lattice profiles for the pixel size of d = 2 mm, for different intra-pixel separations, or pitch p.

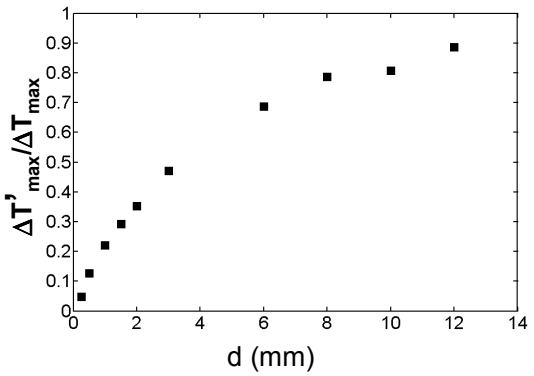

Fig. 11: Peak temperature increase ($\Delta T'_{max}$) at z = 0.5 mm for the same incoming beam fluence, as a function of the incoming spot size d, relative to the peak temperature increase ΔT_{max} when d = 20 mm .

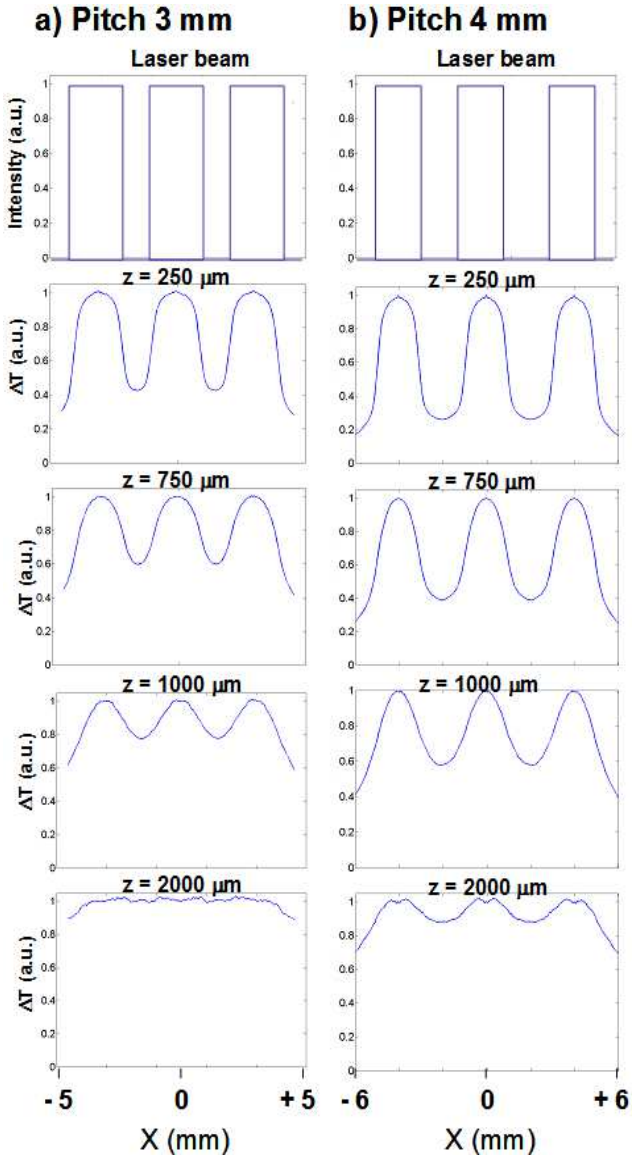

Fig. 12: Calculated temperature profiles within the skin for d= 2 mm pixel spot size, and pixel separations of a) p= 3 mm (40% skin coverage); and b) p= 4 mm (22% coverage).

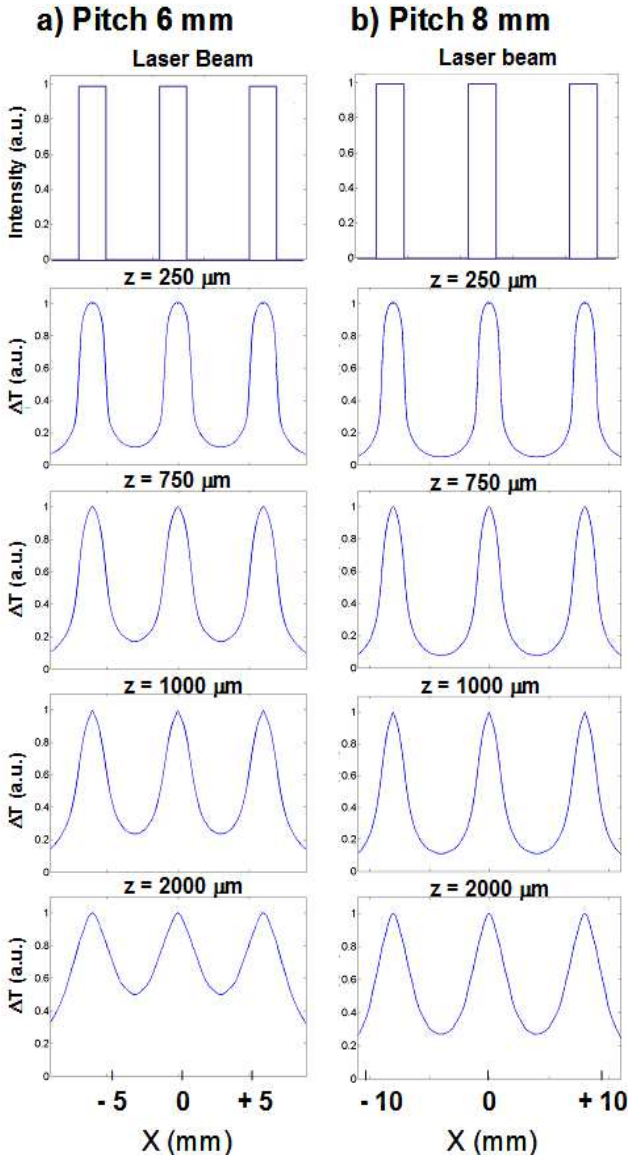

Fig. 13: Calculated temperature profiles within the skin for d= 2 mm pixel spot size, and pixel separations of a) p=6 mm (10% skin coverage); and b) p= 8 mm (6% skin coverage).

IV. DISCUSSION

a) Optimal Nd:YAG fractional spot size

As can be seen from Fig. 11, in order to achieve the same peak temperatures with smaller incoming beam spot sizes, the incoming laser fluence must be increased correspondingly in order to compensate for the effects of scattering. Compared to a very large spot size of 20 mm, the incoming beam fluence must be increased by a factor of almost 3 when a 2 mm spot size is used. For even smaller spot sizes, such as 0.5 mm and 0.25 mm, their fluence must be increased by a factor of 8 and 20, respectively. Extremely small spot sizes are therefore not recommended as the required fluences of the laser beam would be above the levels that are considered safe for the epidermis.

Another reason why extremely small spot sizes are not suitable for use with deeply penetrating laser wavelengths, such as 1064 nm, is the fact that due to scattering, the effective spot size within the skin cannot be reduced below approximately 1.5 mm. This can be seen in Figs. 14 and 15 which shows the dependence of the effective spot size d' on the incoming spot size d, at z = 0.5 mm and z = 1 mm. The effective spot size d' was calculated using:

$$d' = d \sqrt{(\Delta T_{max} / \Delta T'_{max})} \quad (5)$$

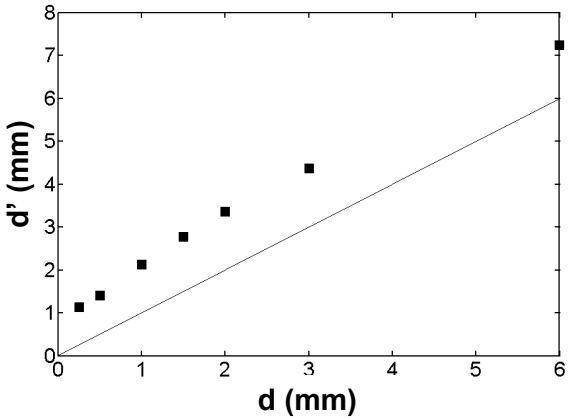

Fig. 14: Effective spot size d' at skin depth of z = 0.5 mm as a function of the incoming beam spot size d. The line shows the effective spot size for the case when there is no scattering.

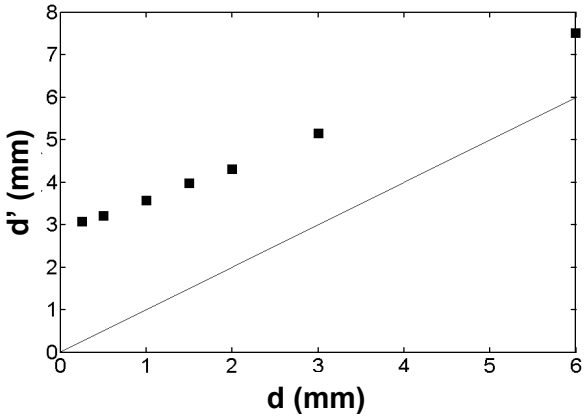

Fig. 15: Effective spot size d' at skin depth of z = 1 mm as a function of the incoming beam spot size d. The line shows the effective spot size for the case when there is no scattering.

When taking into account the diminishing temperatures and beam broadening with smaller spot sizes, a fractional pixel spot size between 1.5 and 2 mm seems to represent an optimal solution for non-ablative fractional Nd:YAG laser treatments. Note that this would not apply if the Nd:YAG laser fluence was increased above the skin's phase transition

temperature or ablation threshold. In such a case, the laser light would "tunnel" through the skin, and the effects of scattering would be considerably reduced.

Figure 16 shows how the effective spot size (d') of the 2 mm incoming beam (d=2mm) increases with skin depth.

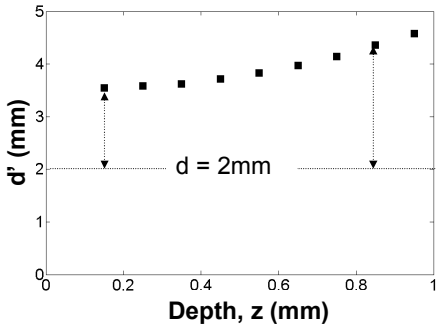

Fig. 16: Effective spot size d' for the incoming beam spot size of d = 2 mm, as a function of skin depth.

The scattering of a d = 2 mm incoming beam close to the skin surface results in a broadened effective spot size of d' = 3.5 mm. The effective spot size remains approximately constant till the depth of z = 0.5 mm, after which it starts to spread faster.

b) Influence of fractional skin coverage on fractional depth

As can be seen in Figs. 12 and 13, when fractional laser pixels are not spaced sufficiently far apart, their broadened temperature profiles within the skin begin to overlap. This leads to a flattening of the temperature profiles and to a less pronounced "temperature lattice". To quantify this effect we define the fractionality F by the ratio of the temperature minimums and maximums in the fractional temperature lattice:

$$F = (\Delta T_{max} - \Delta T_{min})/\Delta T_{max}. \quad (6)$$

Using the numerical model we can then plot the fractionality F as a function of skin depth for different values of skin coverage (See Fig. 17).

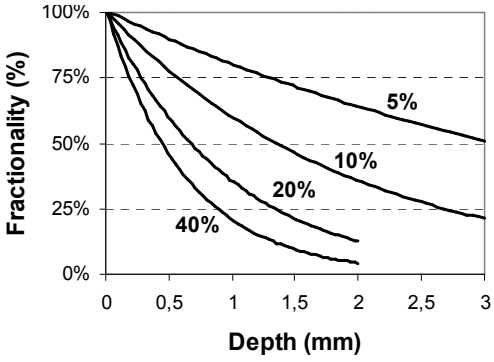

Fig. 17: Fractionality as a function of skin depth (z) for different values of skin coverage. The incoming beam spot size is 2mm.

If we somewhat arbitrarily define that fractional heating is effective only when F > 50%, we can conclude that by varying the skin coverage the operator can vary the fractional depth z_F above which the effect of the Nd:YAG laser light can be considered fractional, and below which the effect can be considered as mostly homogeneous heating of the bulk of the tissue.

For the 2 mm pixel size and skin coverage values which are available with the Fotona S11 scanner, the fractional depth, z_F, depends on the skin coverage as shown in Table 1.

Table 1: Approximate fractional depths z_F for different values of skin coverage available with the Fotona S11 Nd:YAG scanner.

	Skin coverage (%)				
	63	53	20	16	13
z_F (mm)	**0.2**	**0.3**	**0.6**	**0.8**	**1**

c) Clinical experience

Dr. Mark B Taylor, MD has succesfully used the Nd:YAG laser in a small spot manual mode for over 20 years to treat deeper port wine stains. The fractional mode Fotona Nd:YAG laser scanner S11 scanner makes this treatment safer and faster since the scanner lays down a pattern of deeply penetrating small spot 1064 nm light spicules that effectively coagulate the blood vessels in port wine stains and hemangiomas to a deep and more effective level while sparing tissue in between the light spicules for a safer and more permanent cure. Figure 18 shows a clinical example immediately after a single treatment of resistant port wine stain with the S11 fractional Nd:YAG laser.

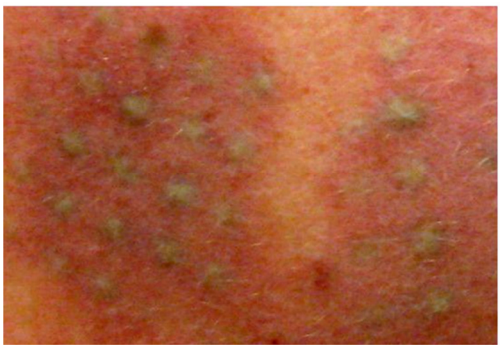

Fig. 18: Treatment of resistant port wine stain with Fotona S11 fractional Nd:YAG scanner: coagulated, darker dots are clearly visible. Laser parameters used were, 20 msec, 160J/cm^2, 2 mm spotsize, 3 mm pitch (20% coverage).

Similarly, Figure 19 shows an intermedium result of resistant port wine stain treatment after the first scanner session.

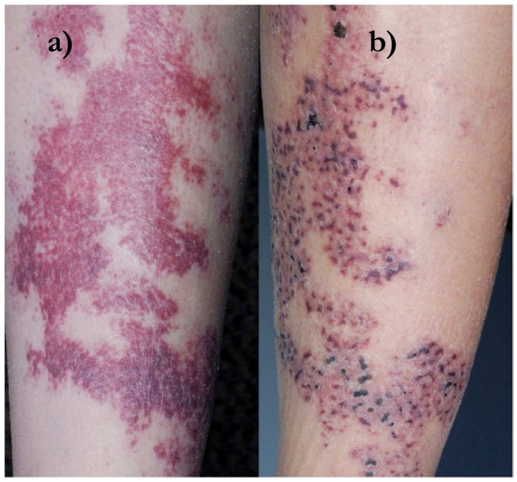

Fig. 19: Treatment of resistant port wine stain with Fotona S11 fractional Nd:YAG scanner: a) before the treatment; b) one month after the first treatment.

Note that multiple treatments (estimated 6 to 10 treatments for most port wine stains) with an interval between the treatments of more than a month are necessary to achieve an optimum result. Also, when multiple passes during one treatment session are administered the overlapping of the spots should be avoided to prevent energy overdosing. A typical outcome of small spots (dotted) treatment is shown on Fig.20.

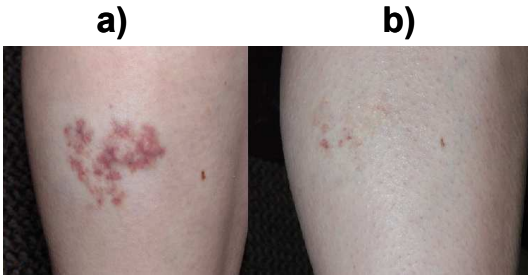

Fig. 20: Succesful treatment of resistant port wine stain with "dotted" technique: a) before the treatment; b) one year after multiple treatments.

V. CONCLUSIONS

In conclusion, using a Monte Carlo numerical model we analyzed the influence of pixel size and skin coverage on the resulting thermal profile within the skin following irradiation with a fractionated Nd:YAG laser beam. It was shown that for deeply penetrating non-ablative laser wavelengths, reducing the pixel size to extremely small spot sizes is not effective. For the Nd:YAG wavelength we showed that the optimal fractional pixel spot size is between 1.5 and 2 mm.

Clinical experience suggests that laser skin treatments, such as treatments of resistant port wine stains and hemagiomas can benefit considerably by using the recently introduced fractionated Nd:YAG scanner (Fotona S11) laser beam technique.

It was also demonstrated that light scattering effects within the skin can be utilized to adjust the skin depth to which the effect of laser light can be considered fractional. A fine tuning of the fractional depth was shown to be achievable with the S11 by a simple adjustment of skin coverage. This effect suggests an interesting and novel concept in non-ablative fractional skin rejuvenation since it is now possible to combine fractional and bulk skin-heating treatments within one treatment session, and with the same laser device.

Acknowledgment

This research was carried out in a collaboration with the EU regional Competency Center for Biomedical Engineering (www.bmecenter.com), coordinated by Laser and Health Academy (www. laserandhealthacademy.com), and partially supported by the European Regional Development Fund and Slovenian government.

REFERENCES

1. Branov E, Tankovich N, Tissue Cooling Rod for Laser Surgery, (section Patterned Cooling Element for Masking Portions of Tissue), US patent 6,632,219. Filed March 10, 2001.
2. Manstein D, Herron GS, Sink RK, et al. Fractional photothermolysis: a new concept for cutaneous remodeling using microscopic patterns of thermal injury. Lasers Surg Med 2004; 34:426-38.
3. RR. Anderson, J.A. Parrish. Selective Photothermolysis-precise Microsurgery by Selective Absorption of Pulsed Radiation, Science 220:524-527 (1983).
4. C. C. Dierickx et al. Micro-Fractional Ablative Skin Resurfacing with Two Novel Erbium Laser Systems, Lasers in Surg. and Med. 40, pp 113-123, 2008.
5. Pozner JN, Glanz S, Goldberg DJ. Fractional erbium resurfacing: Histologic and early clinical experience, Lasers in Surg. and Med. 39, pp S19:73, 2007.
6. Lukac M, Perhavec T, Nemes K, Ahcan U. Ablation and Thremal depths in VSP Er:YAG Laser Skin Resurfacing, J. LAHA, Vol. 2010, No.1: 56-71 (2010). www.laserandhealth.com.
7. Lukac M, Zabkar J, Gorjan M, Vizintin Z, 2010, Beyond Customary Paradigm: Self-Induced Fractional Nd:YAG Laser Hair Removal, J. LAHA, Vol. 2010, No.1: 35-46 (2010) www.laserandhealth.com.
8. FRAC3® is a Fotona trademark (www.fotona.com) for the self–induced three-dimensional fractional treatment approach in laser skin treatments.
9. M. Gorjan, L. Grad, M. Lukac. Three-Dimensional Fractional Laser Skin Rejuvenation, IMCAS 2008 Abstracts Booklet, P28.
10. Lukac M, Sult T, Zabkar J, Gorjan M, Vizintin Z. Parameters for the New FRAC3 Nd:YAG Laser Skin Treatment Modality. J. LAHA, Vol. 2010, No.1: 47-55 (2010). www.laserandhealth.com.
11. Lukac M, Zabkar J, Gorjan M, Sult T. FRAC3: Three-Dimensional Non-Ablative Fractional Laser Skin Rejuvenation. J. Laser Health Academy, 2009(2):20-23. www.laserandhealth.com.

12. Bevec T, Lukac M. Fractional FRAC3 and Twinlight Laser Skin Treatments, J. LAHA, Vol. 2011, No.1: 43-48 (2011). www.laserandhealth.com.
13. S11-F is a fractionated scanning handpiece manufactured by Fotona d.d. www.fotona.com.
14. Markolf H. Niemz. Laser-Tissue Interactions. Springer-Verlag, 1996.
15. A. Ishimaru. Wave propagation and scattering in random media. Academic Press, 1978.
16. Ashley JW, Martin JC van Gemert. Optical-Thermal Response of Laser-Irradiated Tissue. Plenum Press, 1995.
17. Crochet JJ, Gnyawali SC, Lemley YCEC, Wang LV, Chen WR. Temperature distribution in selective laser-tissue interaction. Journal of Biomedical Optics, 11(3), 2006.
18. Wang L, Steven LJ. Monte Carlo Modeling of Light Transport in Multi-layered Tissues in Standard C, 1998.
19. Marini L. Sequential Photothermal 1,064 Nd:YAG and 2,940 nm Er:YAG Fractional Resurfacing and Remodelling versus 2,940 nm Er:YAG Fractional resurfacing Alone: a Comparative Study, Lasers. Surg. Med 2011; 43: 949.
20. Marini L. Thermo-Fractional PDT for Persistent Warts, Lasers. Surg. Med 2011; 43: 939.
21. Marini L. Sequential Photothermal 1,064 Nd:YAG and 2,940 nm Er:YAG Fractional Resurfacing and Remodelling versus 2,940 nm Er:YAG Fractional resurfacing Alone: a Comparative Study, J. LAHA, Vol. 2011, No1. www.laserandhealth.com.
22. Marini L. Twinlight Rejuvenation Technique (Nd:YAG+Er:YAG) vs Er:YAG Resurfcaing Alone: a Comparative Study, J. LAHA, Vol. 2011, No1. www.laserandhealth.com.